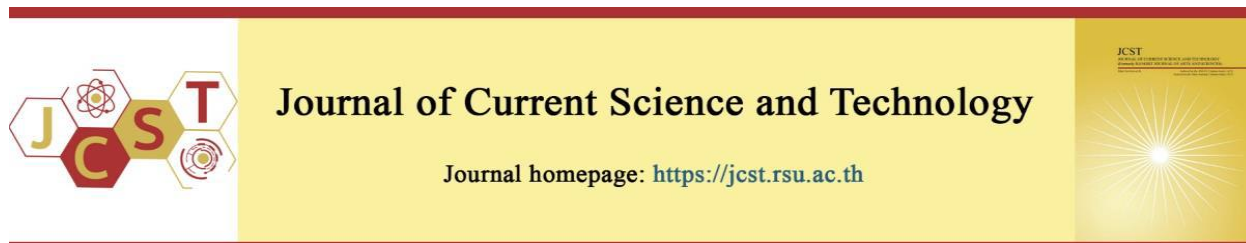


Cite this article: Pumpuang, A., & Aobpaet, A. (2024). Evolution pattern of land subsidence using InSAR time-series analysis in Bangkapi, Bangkok, Thailand. *Journal of Current Science and Technology*, 14(3), Article 49.
<https://doi.org/10.59796/jcst.V14N3.2024.49>



Evolution Pattern of Land Subsidence Using InSAR Time-Series Analysis in Bangkapi, Bangkok, Thailand

Angkana Pumpuang, and Anuphao Aobpaet*

Department of Civil Engineering, Faculty of Engineering, Kasetsart University, Bangkok 10900, Thailand

*Corresponding author; E-mail: fengaha@ku.ac.th

Received 10 October 2023; Revised 31 March 2024; Accepted 2 April 2024
Published online 1 September 2024

Abstract

Subsidence in Bangkok has occurred continuously for a long time. This research applied radar satellite imagery (Sentinel-1 101 images, 2017–2022) to track land subsidence using the time series INSAR technique. The study area was in the Bang Kapi area in Bangkok, which has a high level of cumulative subsidence. The pattern of cumulative subsidence change was analyzed using the standard deviation ellipse (SDE) technique. The results showed that the Bang Kapi area had the highest cumulative subsidence in 2019 (-125.31 mm). The movement of the subsidence center changed every year in different directions with three patterns identifiable. The first pattern showed the evolution of subsidence in a northeast-southwest direction, the second pattern showed subsidence evolution in a northwest-southeast direction, and the third pattern presented evolution that did not appear to be in any specific direction. The size of the subsidence area in 2017 and 2022 increased, whereas between 2018 and 2021, the subsidence area decreased compared to other years during the research period.

Keywords: *InSAR; PSInSAR; time-series; cumulative subsidence; SDE*

1. Introduction

Interferometric synthetic aperture radar (InSAR) was first reported in the late 1990s (Rosen et al., 2000). It is a powerful technique for mapping land movement tracking by taking advantage of microwave reflections sent by radar satellites. The radar system can measure changes regularly according to the satellite's orbital cycle. Although the InSAR technique is very appropriate, it has some limitations regarding temporal decorrelation and atmospheric dispersion, including for the troposphere and ionosphere (Ding et al., 2008). Later, InSAR was developed into the Persistent

Scatterer InSAR (PSInSAR) technique (Ferretti et al., 2001) to overcome the above restrictions of the InSAR technique. This latter technique provided better results and could track changes or movements in various areas of terrain, such as landslide monitoring (Hussain et al., 2021; Rosi et al., 2018; Sun et al., 2015), earthquakes (Dumka et al., 2020; Lu et al., 2007), movement due to volcanic eruptions (Gatsios et al., 2020; Hooper et al., 2004; Pritchard, & Simons, 2004), and land subsidence monitoring (Zuo et al., 2019). InSAR provides high accuracy to the cm or mm level when calibrated with higher resolution instruments, such as scales or GNSS

(Cigna et al., 2021; Fuhrmann et al., 2015; Yang et al., 2016). Therefore, the PSInSAR technique is globally accepted, especially because of its effectiveness in detecting changes in the land surface or subsidence over large areas. Many studies have successfully used the INSAR technique as a subsidence monitoring tool (Khan et al., 2022; Li et al., 2021; Ramirez et al., 2022; Sousa et al., 2008; Sun et al., 2017)

In 1968, the first research was reported by Cox (Phien-wej et al., 2006) regarding the subsidence in Bangkok Metropolis and surrounding provinces. The report showed that the main factor causing subsidence was groundwater pumping, as many sectors needed water for consumption, including agriculture and the industrial sector. However, there was insufficient tap water to meet the demand. Groundwater is another exploitable water resource. When removal (for example, by pumping) of the massive quantity of groundwater is greater than the amount of water recovered, piezometric levels (underground pressure) will decrease in the clay and aquifers layers, which may significantly cause soil erosion (Babel et al., 2006). In addition, the alluvial characteristics of the soil in Bangkok and the surrounding river delta area make it prone to subsidence. Eventually, land subsidence in the Bangkok Metropolis area reached a crisis level.

The initiative to monitor subsidence in Bangkok and its metropolitan regions commenced in 1983 under the auspices of the Royal Thai Survey Department, utilizing the first-order leveling method known for its high precision. This methodology facilitated a thorough assessment of subsidence phenomena. The Royal Thai Survey Department categorized the surveyed areas into three tiers based on the severity of subsidence: Critical Zone Stage 1, characterized by a subsidence rate exceeding 10 cm per year; Critical Zone Stage 2, exhibiting a subsidence rate between 5 and 10 cm per year; and Critical Zone Stage 3, demonstrating subsidence below 5 mm per year. Utilizing the traditional leveling approach, the Bang Kapi area was identified as falling within critical zone stage 1, indicating significant subsidence. Notably, data spanning from 1978 to 2007 revealed that certain regions within Bang Kapi experienced substantial subsidence accumulation, reaching up to 108 cm (Department of Groundwater Resources, 2012). Despite the method's commendable precision, its implementation is constrained by substantial financial requirements and

extensive operational time needed for large area coverage, necessitating a considerable allocation of equipment and human resources for surveying. Consequently, the periodic nature of survey operations impedes yearly subsidence monitoring.

Interferometric Synthetic Aperture Radar (InSAR) emerges as a viable alternative for continuous monitoring of land changes, offering the advantage of cost-effectiveness and wide coverage. Numerous successful endeavors have utilized the InSAR technique to discern land subsidence patterns in Bangkok and its adjacent regions. For instance, a study (Kun et al., 2004) conducted in 1999 leveraged InSAR in conjunction with images acquired from the ERS1/2 radar satellite to gauge subsidence levels. The methodology involved computing the phase disparity between two distinct time intervals, specifically December 21 and 22, 1999. The outcomes delineated a comprehensive map depicting subsidence occurrences in Bangkok and its environs, exhibiting enhanced accuracy in the spatial distribution of subsidence data compared to conventional benchmark leveling measurements. Additionally, a subsequent investigation capitalized on 19 Radarsat-1 images spanning from October 2005 to March 2010 (Aobpaet et al., 2013). Employing the Combined Persistent Scatterer Interferometry (PSInSAR) and Small Baseline (SB) methodological approach, this study discerned subsidence rates ranging between 10 to 30 mm per year within the Bangkok area, further highlighting the efficacy of InSAR in delineating temporal subsidence trends.

Based on the research review, the INSAR technique can be analyzed using imagery from various radar satellites. Each satellite exhibits distinct properties including resolution, revisit time, and wavelength. Radar wavelengths are categorized into four types: C-band, X-band, P-band, and L-band. The C-band, with radar wavelengths ranging from 3.8 to 7.5 cm and medium frequency, possesses the capability to penetrate medium-sized vegetation, making it well-suited for urban change monitoring. Prominent radar satellites operating in the C-band wavelength include Sentinel-1 and RADARSAT-2. The X-band radar wavelength, shorter than the C-band, spans from 2.4 to 3.8 cm and has a high frequency. TerraSAR-X is an exemplar of a radar satellite operating within this wavelength range. Its capacity to penetrate low vegetation is notable, with a majority of reflections redirected to the vegetation's

top layer and limited ground penetration. This characteristic renders it particularly suitable for monitoring ice, snow, and climatic conditions. The P-band, operating within a wavelength range of 30 to 100 cm and featuring a low frequency, is exemplified by satellites such as AIST-2. It demonstrates proficiency in penetrating vegetation, making it suitable for tracking changes such as deforestation and agricultural applications. The L-band, with wavelengths ranging from 15 to 30 cm and characterized by a low frequency, exhibits enhanced penetration capabilities through vegetation and is therefore adept at measuring land changes in vegetated regions. Satellites equipped with L-band sensors, including ALOS and NISAR, facilitate comprehensive monitoring of vegetative dynamics and land surface alterations.

The study indicated that the choice of radar band type is contingent upon the specific characteristics of each area and the objectives of the research. In the context of this study, which aims to monitor subsidence in Bangkok, a predominantly urban area, the use of the C-band suffices for processing purposes as it does not necessitate excessively long wavelengths to penetrate the canopy effectively. Sentinel-1 stands out as an attractive satellite option due to its provision of a free C-band sensor. Moreover, the availability of historical data dating back to 2012 enables the tracking of past subsidence trends, while its recurring orbital cycle, featuring a revisit time of 12 days and a resolution of 10 meters, facilitates the continuous monitoring of future subsidence. Consequently, the Sentinel-1 satellite is deemed suitable for monitoring land subsidence dynamics in the Bangkok area.

Therefore, this research investigated how the current subsidence pattern in the Bang Kapi district has changed during the study period. The results of the study should provide information to support relevant agencies in adjusting action response plans or issuing measures to solve the subsidence problem. At this stage, there have been no published research studies on the characteristics or patterns of land subsidence in the study area. Consequently, this research focused on subsidence patterns using the PSInSAR technique, cumulative subsidence, and the standard deviation ellipse (SDE) during 2017–2022 in Bang Kapi, Bangkok.

2. Objectives

The major purpose of the research is to generate a cumulative land subsidence map in Bangkok, Bangkok, Thailand from Sentinel-1 SAR images using the PSInSAR time-series algorithm and to study evolution pattern of subsidence by using the standard deviation ellipse (SDE). The pattern can be divided according to the severity of the cumulative subsidence into three types: small level (-60 to -80 mm), medium level (-80 to -100 mm), and high level (-100 mm).

3. Materials and methods

3.1 Study area

Bangkok, the capital of Thailand, is located in the lower central region of the country (coordinates 13.45 degrees N; 100.28 degrees E) with a total area of approximately 1,500 sq. km, consisting of 50 administrative districts (Figure 1). The topography is a river basin that drains into the Gulf of Thailand. The soil is characterized as a soft clay called 'Bangkok clay'. The Chao Phraya River is the main drainage path that flows through Bangkok, providing the boundary between western Bangkok and eastern Bangkok.

Bang Kapi district is one of the important districts in Bangkok, located in the eastern part of the city. It is the center of economic, educational, and residential activities. The Bang Kapi district consists of 2 subdistricts: Khlong Chan in the north and Hua Mak in the south. Bang Kapi district has an area of approximately 28.5 sq. km, with many canals flowing through it. In the past, most of the area was agricultural land, which has been transformed into villages and buildings. Urban expansion has increased to accommodate the growing number of people traveling to work or living there.

3.2 Radar dataset

This research used images from Sentinel-1, a resource-sensing satellite operated by the European Space Agency. The satellite is fitted with a C-band antenna with a wavelength of 5.6 cm and has a sun-synchronous orbit that repeats every 12 days. The current research used data from path 62 frame 545, covering the lower central region of Thailand (Figure 2). Based on the EPSG 4326 geoid, the latitude and longitude, of the image corners, respectively, were: top left corner 12.97, 101.28; top right corner 13.34, 99.01;

bottom right corner 15.00, 99.33; and bottom left corner 14.57, 101.62. Interferometric wide swath (IW) mode is a pre-defined mode suitable for tracking land or coastal changes. The data capture area capacity, or swath width, is 250 km. The single look complex (SLC) level contains three sub-swaths consisting of IW1, IW2, and IW3. The incident angle is approximately 29.1–46.0 degrees. The current study analyzed 101 images of

Sentinel-1 radar satellite image data captured between October 13, 2017, and June 1, 2022. The image date of July 9, 2019 was selected as the master image because it provided a minimum temporal interval, a choice made to optimize coherence and mitigate terrain motion effects during the generation of interferograms for a total of 100 image pairs.

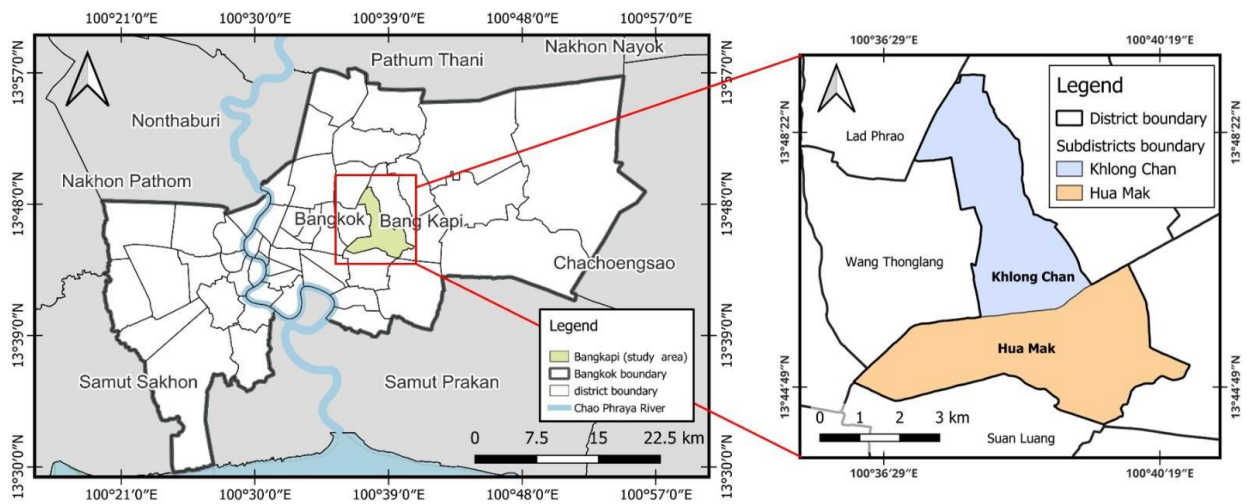


Figure 1 Study area

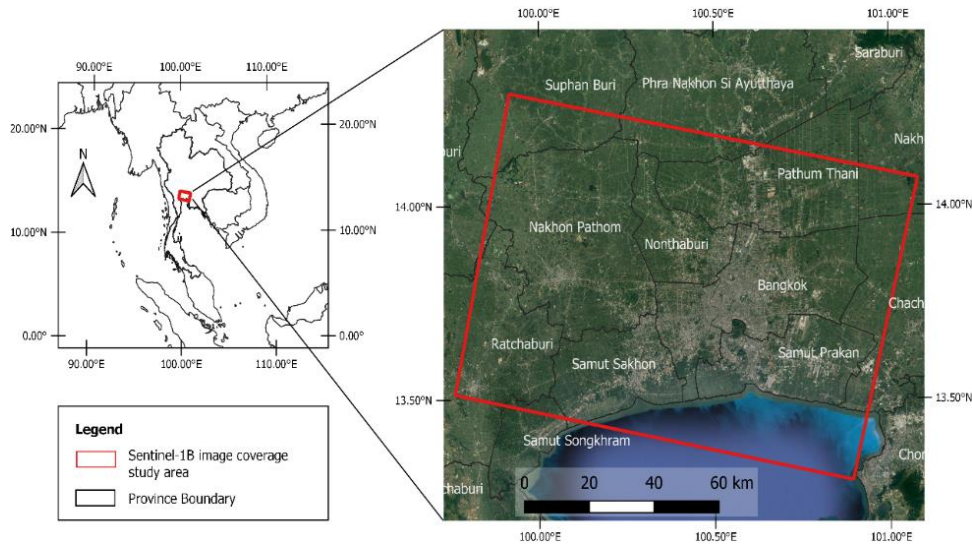


Figure 2 Coverage of Sentinel-1 scene (path 62 frame 545)

3.3 Processing radar images based on the PSInSAR time series algorithm

This processing contained two steps: 1) pre-processing data and generating interferograms; and 2) processing the PSInSAR time series, as follows:

3.3.1 Pre-processing data and generating interferograms

This step was accomplished using the Sentinel Application Platform (SNAP) software, developed by Brockmann Consult, SkyWatch, and C-S. SNAP is a sentinel satellite toolbox for processing observation satellite datasets and additionally supports images from Sentinel-1. It is efficient in pre-processing and generating interferograms.

Many successful studies have used SNAP to create interferograms. For example, Jennifer et al., (2022) processed 19 Sentinel-1 images in 2020 to create 18 pairs of interferograms to analyze and monitor landslides in Kerala, India. Furthermore, Foumelis et al., (2018) processed land subsidence using SNAP to create interferograms for studies in Mexico City, Mexico and Rome, Italy. However, the SNAP software has limited processing capabilities, requiring at least 16 GB of RAM due to the massive amount of raw satellite data. If the RAM is smaller than this, the processing will take a long time or may not even be possible.

The pre-processing step involved selecting data areas to cover the study area. This research selected data from path 62 and frame 545, using IW mode and the SLC product, covering an area of 250 sq. km in lower central Thailand. The Sentinel-1 IW mode is divided into three sub-swaths (IW1, IW2, and IW3), and a sub-swath contains nine parts. The researcher chose IW1 and IW2 with sub-swathes 4–9 and 5–8, respectively, because the aforementioned data properties were suitable for Bangkok. The researcher applied co-registration processing to ensure that targets in slave images had the same range and azimuth as the master image by selecting the data region similarly to IW and sub-swath locations.

The next step was satellite orbit adjustment using the apply orbit file function. Generally, the SAR image contains orbit metadata information, which is not highly accurate. This was addressed by receiving highly accurate satellite orbit data in precise orbit ephemerides (POE) files from the Precise Orbit Determination Service. This step downloaded POE data automatically. If no POE data

were found, the orbit data was selected for processing instead. However, the accuracy may then be lower than for processing with POE data.

Next geometry from topographic maps was applied to the range and azimuth direction of the images. In this case, the geometry was SRTM 3 sec DEM (Shuttle Radar Topography Mission 90 m, digital elevation model), with the bilinear interpolation method used for interferometric phase simulation.

Next, the multiple bursts of the Sentinel-1 images were combined into a single image using the deburst operation on every image.

An interferogram can be processed by using a master image paired with a slave image. Each interferogram image is produced by multiplying the conjugate of the complex numbers of the master and slave images. Then, the SRTM 90 m DEM was applied to remove the topographical phase. The DEM was converted to radar coordinates and subtracted from the interferogram as a differential interferogram.

The final step of the interferogram processing before transfer to the PSInSAR time series method involved the StaMPS export operator. The persistent scatter InSAR (PSInSAR) method was selected to export the co-registration stack and elevation interferogram data.

3.3.2 PSInSAR time-series processing

StaMPS is open-source software developed by Stanford University. It is effective in PSInSAR, SB (small baseline), and mixed algorithms. Many studies around the world have successfully used StaMPS for land deformation monitoring, such as a study (Sun et al., 2015) that processed 16 ALOS/PASAR images in January 2015, and from 2007 to 2010 to study landslides in Zhouqu, China, using the StaMPS-SB algorithm. Later, Sousa et al. (2011) used data from three satellites (ENVISAT ASAR, RadarSat-2, and TerraSAR-X) from 2004 to 2013 covering the Beijing area, China, and selected the PSInSAR time-series algorithm in StaMPS to successfully track land subsidence in the study area.

Initially, the PSInSAR time-series algorithm is applied, which is a batch script execution in the INSAR master folder that increases the number of patches in the range and azimuth of the interferogram data. Generally, each patch should have less than five million SLC pixels. This process decreases the data size and facilitates its management within the constraints of computer

memory to allow successful processing. Next, processing with the PSInSAR time-series algorithm involves using the StaMPS, which must integrate with the Matlab software.

This is followed by loading the data and converting it into Matlab formats for storage in the workspace. Then, the phase estimation occurs for each candidate pixel in every interferogram. The density per sq. km of non-PS (Persistent scatterer) pixels is then estimated. PS weeding is a procedure that eliminates random phases caused by excessive noise from signal components. Phase correction combines the individual patches, with the PS pixels selected from the wrapped phase, are corrected using the spatially uncorrelated look angles method. Then, phase unwrap estimates the error in the spatially uncorrelated look angle. The last processing step of the PSInSAR algorithm is atmospheric filtering, after which the algorithm generates output data as the deformation rate in the line of sight to create a map and export the data as .csv file.

3.4 Cumulative subsidence analysis

This process is the evolution pattern of cumulative subsidence analyses in the study area based on calculating the sum of the vertical changes in the time study period. For example, the cumulative value for 2017 is the sum of all vertical displacement data in that year in the study area. Next, the cumulative displacement for 2018 is the sum of vertical displacement data in from 2017 through to the end of 2018. In this context, 'cumulative subsidence' refers to a negative value of cumulative displacement. The result presents a cumulative subsidence map that displays only points that have significant cumulative values of less than -60 mm. If the point value exceeds the specified limit, it is eliminated from the map.

3.5 Standard deviation ellipse

The standard deviation ellipse (SDE) was first introduced by Lefever (1926) to characterize the distribution of geographic components (Figure 3). This method describes the spatial distribution and can identify the trend direction of geographical phenomena. The long axis of the ellipse represents

the direction of the gravity center, while the short axis refers to the discontinuous direction of the gravity center. If the ellipse is inclined more in one direction, then the objects distribute clearly in that direction (Peng et al., 2016). Equation (1) and equation (2) are used to calculate the center of the SDE in the x-axis dispersion and the y-axis dispersion, respectively (Guo et al., 2021):

$$SDE_x = \sqrt{\frac{\sum_{i=1}^n (x_i - \bar{X})^2}{n}} \quad (1)$$

$$SDE_y = \sqrt{\frac{\sum_{i=1}^n (y_i - \bar{Y})^2}{n}} \quad (2)$$

where x_i and y_i denote the positions of point i in the x-axis and the y-axis, respectively, and n denotes the total number of points. Equation (3) is used to calculate azimuth:

$$\tan\theta = \frac{(\sum_{i=1}^n x_i^2 - \sum_{i=1}^n y_i^2) + \sqrt{(\sum_{i=1}^n x_i^2 - \sum_{i=1}^n y_i^2)^2 + 4(\sum_{i=1}^n \bar{x}_i \bar{y}_i)^2}}{2 \sum_{i=1}^n \bar{x}_i \bar{y}_i} \quad (3)$$

Equation (4) and equation (5) calculate the standard deviation of the x and y axes, respectively:

$$\sigma_x = \sqrt{\frac{\sum_{i=1}^n (\bar{x}_i \cos\theta - y_i \sin\theta)^2}{n}} \quad (4)$$

$$\sigma_y = \sqrt{\frac{\sum_{i=1}^n (\bar{x}_i \sin\theta - y_i \cos\theta)^2}{n}} \quad (5)$$

where θ refers to the azimuth angle of the ellipse, which is expressed as the angle formed by rotating clockwise from north to the principal axis of the ellipse, and σ is the standard deviation.

In this research, the ellipse indicates the spatial boundary and shape characteristics of the subsidence in the study area. The indicators illustrate the average spatial center, the major and minor axes of the SDE (corresponding to the intensity of the dispersion geographic points), and the azimuth represents the main trend direction.

For simplicity, the research method — processing radar images based on the PSInSAR time-series algorithm (section 3.3), cumulative subsidence analysis (section 3.4), and standard deviation ellipse (section 3.5)—are compiled into a workflow, as shown in Figure 4.

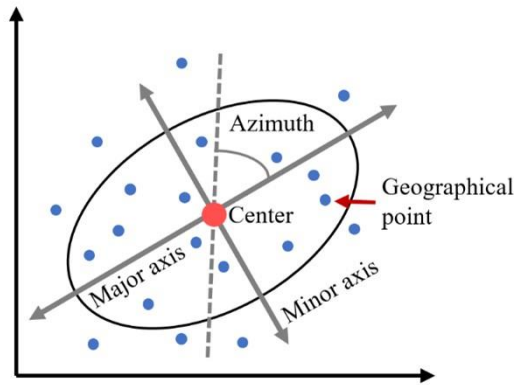


Figure 3 Standard deviation ellipse components: modified from Li et al., (2017).

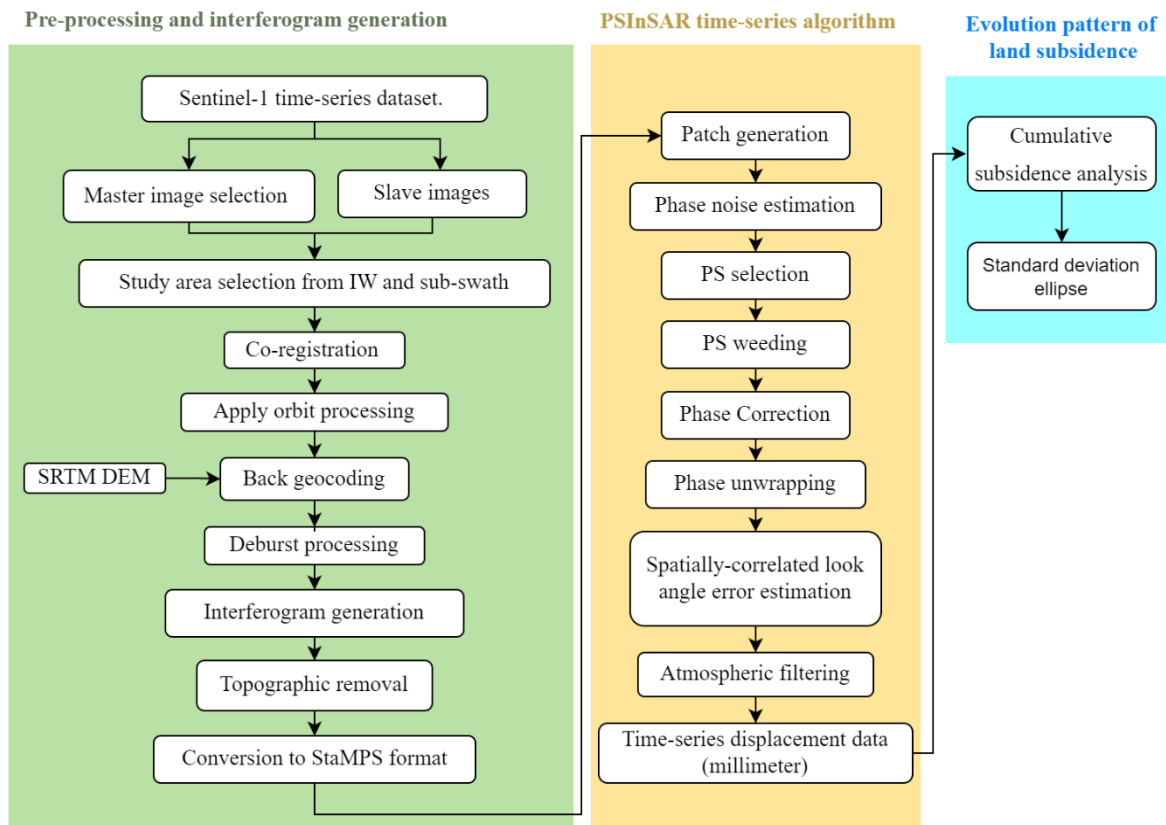


Figure 4 The evolution pattern of land subsidence using InSAR time-series analysis workflow

4. Results

4.1 Accuracy assessment

This study assesses the accuracy of Interferometric Synthetic Aperture Radar (InSAR) data by comparing it with ground truth measurements, including leveling and Global Navigation Satellite System (GNSS), to confirm its reliability for monitoring land deformation. Utilizing data from the GNSS Continuously Operating Reference Stations (CORS) of the Royal Thai Survey Department, specifically the SBKK station, spanning five months from October 2019 to February 2020. Despite the unavailability of InSAR data at the SBKK location, a buffer with a radius of 100 meters was generated to store InSAR time series within proximity. The average vertical change within this buffer was calculated. A linear regression 1:1 graph was plotted to compare GNSS and InSAR data (Figure 5), revealing a maximum difference of 9.76 mm and a minimum of 0.1 mm. The correlation coefficient (R-value) was determined to be 0.88, with a root mean square error (RMSE) of 3.98 mm. These findings suggest that the data obtained through the PSInSAR time-series process effectively monitors land deformation changes.

4.2 InSAR time-series data and cumulative displacement

The results of InSAR processing revealed time-series millimeter data spanning from 2017 to 2022 in the Bang Kapi area, enabling an analysis of data distribution characteristics. Boxplot techniques were employed to compare the annual average subsidence, as illustrated in Figure 6. It was observed that in 2017, the area experienced the highest subsidence compared to other years, with vertical changes ranging from -36.5 to -2.31 mm and an average subsidence of -20.09 mm. Conversely, in 2018, there was a higher uplift resulting in a combination of subsidence and uplift values, ranging from -9.94 mm to +3.46 mm, with an average of -2.31 mm. Subsequently, from 2019 to 2021, a trend of slight subsidence and recovery was noted, with values clustered near zero and similar average magnitudes. Specifically, the years 2019, 2020, and 2021 exhibited average values of -0.08 mm, +1.65 mm, and +0.86 mm, respectively. Notably, in 2022, a marginal increase in subsidence was observed, with an average value of -5.36 mm. These findings offer insights into the temporal dynamics of land subsidence in the Bang Kapi area over the studied period.

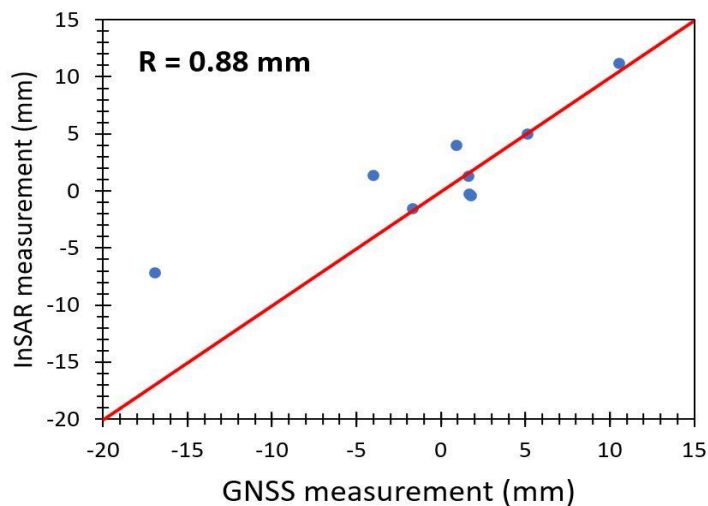


Figure 5 The comparison between GNSS and InSAR data

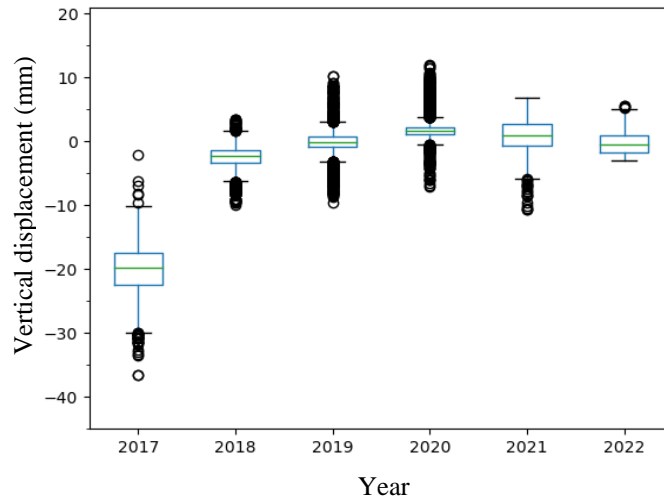


Figure 6 The boxplot of average subsidence (mm) of all points in Bangkapi

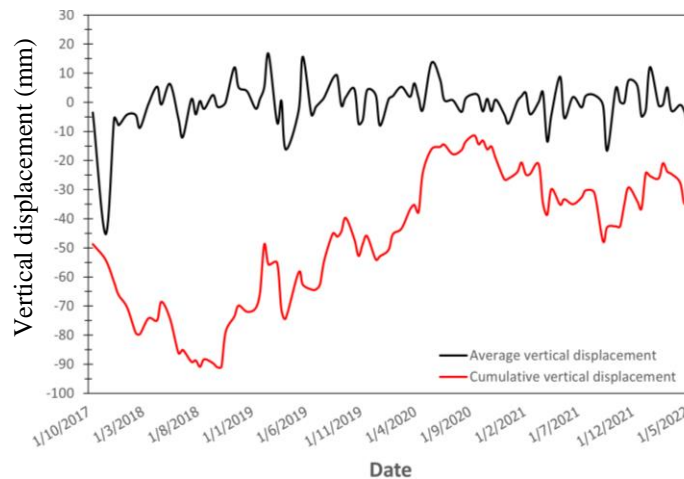


Figure 7 The relationship between average vertical displacement and cumulative vertical displacement in Bangkapi

Figure 7 illustrates the average vertical displacement (represented by the black line) derived from the averaged data of all points within the Bang Kapi area over various periods spanning from 2017 to 2022. The result reveals that in 2017, the region experienced the highest degree of subsidence within the range of -5 to -45 mm. Subsequently, in early 2018, there was a notable uplift from -45 mm, gradually recovering to approximately -5 mm. From the middle of 2018 until 2022, the data exhibited consistent yet minor fluctuations, with values fluctuating between -15 and +15 mm. However, solely considering the average change may obscure underlying trends in the data. Therefore, the research employed the cumulative method for further analysis, represented by the red line in Figure 7. The

cumulative analysis reveals a distinct pattern of pronounced cumulative subsidence from 2017 to early 2019, amounting to -91.05 mm. Subsequently, the land underwent a phase of recovery, reaching its peak elevation in September 2020 (-11.37 mm). Following this peak, the cumulative subsidence curve exhibited a downward trend, indicating the likelihood of further subsidence from October 2021 to December 2021, albeit at a reduced magnitude compared to the initial subsidence period. Notably, in January 2022, the cumulative subsidence curve displayed an upward trend before declining again in June 2022. These findings provide valuable insights into the temporal dynamics of land displacement in the Bang Kapi area, highlighting periods of both subsidence and recovery over the analyzed timeframe.

4.3 Standard deviation ellipse analysis

The SDE is a powerful technique for the accurate representation of delineated geographic features using spatial statistical methods to describe phenomena. This research applied the standard deviation ellipse technique to analyze spatial data,

using land subsidence as the weight, with the results as shown in Figure 8. The map displays cumulative values less than -60 mm, indicating cumulative subsidence of more than 60 mm and also illustrates the shape of the SDE.

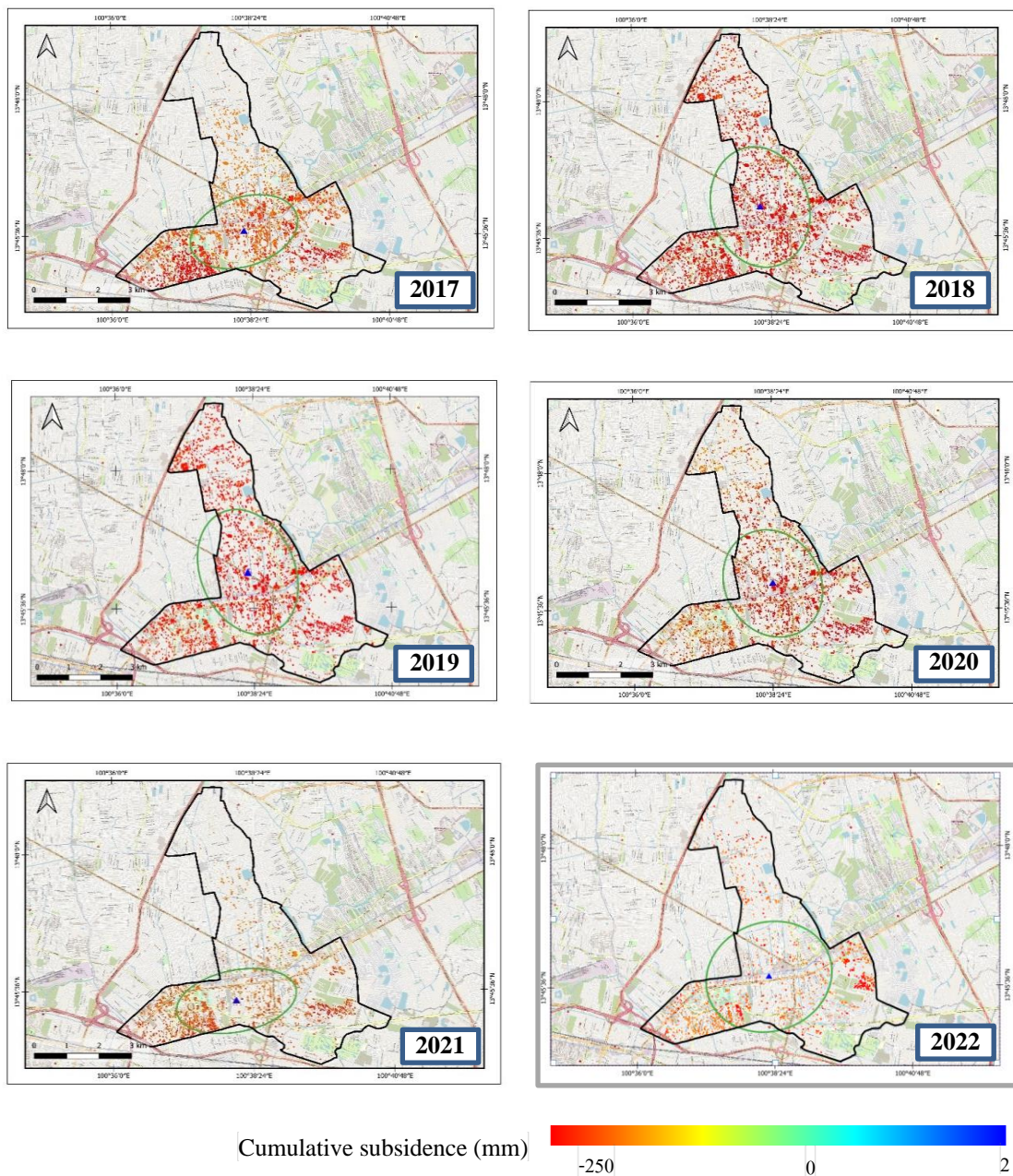


Figure 8 Cumulative subsidence during study period

Figure 8 shows that the cumulative subsidence (mm), the size and shape of the SDE in the Bang Kapi area changed every year from 2017 to 2022 because the development and distribution of the subsidence differed. In 2017, the average cumulative subsidence in the Bangkok was -80.51 mm. The axial direction of the SDE was located in a northeast-southwest direction, indicating that subsidence occurred more in the Hua Mak subdistrict than in the Khlong Chan subdistrict.

By 2018, subsidence was distributed throughout the study area and was more severe compared to 2017. The average cumulative subsidence in the Bangkok was -119.38 mm which increased from 2017. Additionally, the axial shape of the SDE was completely different in 2018, being in a northwest-southeast direction, indicating that the subsidence in 2018 developed and spread more in the north than in 2017.

The years 2019 and 2020 had SDE axes similar to 2018, in a northwest-southeast direction. However, the density distribution of the subsidence points was less than in 2018, indicating that the severity of subsidence had decreased. The average cumulative subsidence in Bangkok was -125.31 mm and -99.38 mm in year 2019 and 2020, respectively.

In 2021, the subsidence was significantly less than in 2020, and the SDE axis aligned in a northeast-southwest direction, indicating reduced subsidence in the north compared to the east-west direction. The average cumulative subsidence in the Bangkok was -74.86 mm in year 2021, which was the least subsidence in study period. This occurrence was indicated that some area was rebound when compared to other study year.

Finally, 2022 experienced the most severe subsidence during the study period, as indicated by the circular shape of the SDE, which was clearly different from other years' shapes. The average cumulative subsidence in the Bangkok was -79.26 mm which was a slight increase from 2021.

In order to conduct a comprehensive investigation into the evolutionary patterns using the SDE method, the level of subsidence was stratified into three categories to generate SDE ellipses, as depicted in Figure 9: small level (green ellipse)

representing cumulative subsidence values ranging from less than -60 mm to -80 mm, medium level (yellow ellipse) indicating cumulative subsidence values from less than -80 mm to -100 mm, and high level (red ellipse) denoting cumulative subsidence values less than -100 mm. Analysis of the SDE shapes revealed distinct spatial patterns across different time periods.

In 2017, the distribution of cumulative low subsidence exhibited a nearly circular shape, suggesting uniform subsidence in all directions. However, moderate and high levels of cumulative subsidence exhibited oval shapes concentrated in the northeast-southwest direction, particularly within the Hua Mak Subdistrict.

Subsequently, in 2018, both cumulative low and moderate subsidence showed a directional trend oriented along the north-south axis, indicating intensified subsidence in the Hua Mak Subdistrict. Conversely, the high level of cumulative subsidence displayed a shape resembling a circle.

In the following year, 2019, the spatial distribution of cumulative low and moderate subsidence maintained a north-south axis alignment similar to that observed in 2018. However, the high level of cumulative subsidence exhibited a shift in distribution pattern towards the southeast-northwest direction.

By 2020, the shapes and axial orientations of cumulative low, medium, and high subsidence levels closely resembled those observed in 2019.

In 2021, a notable divergence in axial orientations was observed across all three levels of cumulative subsidence compared to the previous year. Interestingly, all levels exhibited an east-west axis alignment, indicating a shift in subsidence occurrence towards the Hua Mak area over Klongchan.

Finally, in 2022, the SDE shapes of cumulative subsidence across all three levels appeared nearly circular, suggesting a diffuse spread of subsidence with no clear directional preference.

These results offer significant insights into the temporal and spatial fluctuations of subsidence patterns within the investigated area throughout the analyzed period.

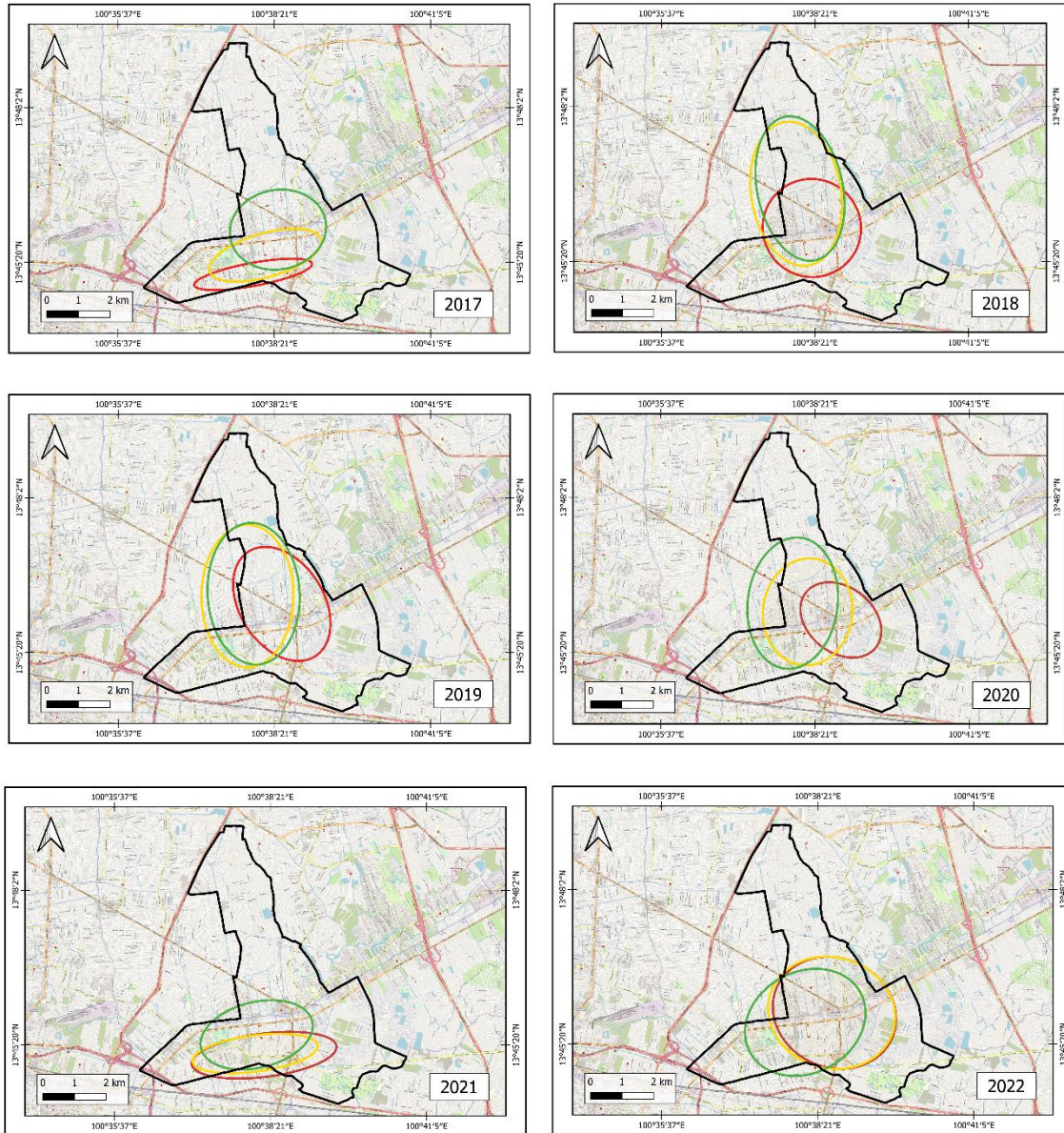


Figure 9 The SDE (green, yellow, and red representing cumulative difference levels categorized as small (green ellipse), medium (yellow ellipse), and high (red ellipse), respectively.)

Figure 10 shows the changes in the area of subsidence in the Bang Kapi area by analyzing the SDE based on cumulative subsidence points. The results show that the subsidence increased in 2018 and 2022 and decreased from 2019 to 2021, with details as follows.

In 2017, the SDE shape had an area of 6.02 sq. km, representing 21.11 percent of the total study area, while the Bang Kapi district had a total area of 28.52 sq. km.

In 2018, the subsidence area increased to 9.44 sq. km, or 33.10 percent of the study area.

In 2019, the subsidence decreased compared to 2018, with subsidence accounting for an area of 9.07 sq. km or 31.80 percent of the study area.

In 2020, the subsidence area continued to decrease, accounting for 8.35 sq. km, representing 29.28 percent of the study area.

In 2021, the subsidence decreased to its lowest level between 2017 and 2022, accounting for an area

of 5.82 sq. km, or 20.4 percent. This phenomenon shows that the points of subsidence are less dispersed.

In the final year, 2022, the subsidence increased to a maximum of 10.86 sq. km of the study area. This showed that the subsidence was more dispersed than in other years.

The center of land subsidence change in the Bang Kapi area is shown in Figure 11—from 2017 until 2022, the center of subsidence based on the SDE method constantly changed position.

In 2017, the coordinates of the center of the SDE were 100.6381 N, 13.7609 E. Later, between 2017 and 2018, the center of the SDE moved to the northwest and then from 2018 to 2019, the center's coordinates repositioned to the northeast. From 2019 to 2020, the subsidence center was displaced to the southeast. Later, between 2020 and 2021, the center again changed its position to the southwest. Finally, from 2021 to 2022, it moved to the northeast (100.6384 N, 13.76281 E).

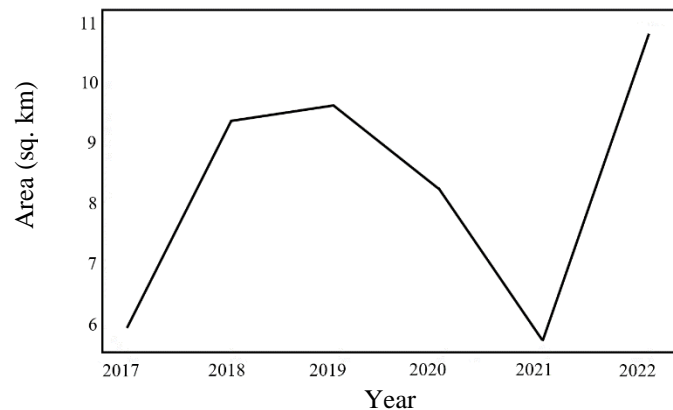


Figure 10 Land subsidence area changes in Bang Kapi area.

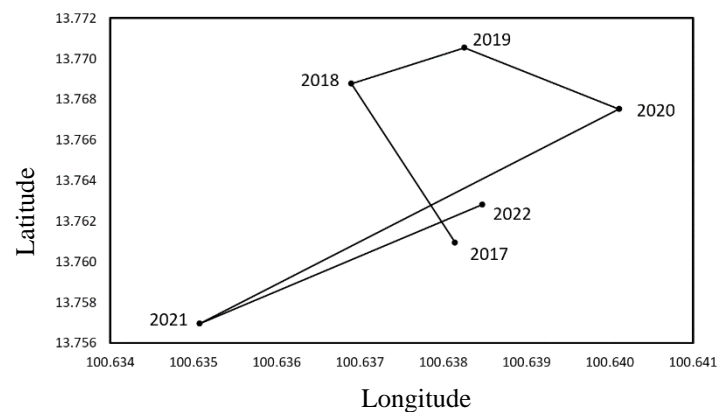


Figure 11 Center of land subsidence change in Bang Kapi area using standard deviation ellipse method.

5. Conclusion

This research studied the pattern of land subsidence in a subset of the Bangkok area using remotely sensed data from 101 Sentinel-1 radar satellite images from 2017 to 2022 based on the PSInSAR technique. The cumulative land subsidence change was calculated using a time-series, with the SDE method applied to analyze the spatial evolution pattern. Subsidence evolution in the study area between 2017 and 2022 could be divided into three patterns:

- 1) Subsidence in a northeast-southwest direction, which occurred in 2017 and 2021.
- 2) Subsidence in a northwest-southwest direction, occurring between 2018 and 2020.
- 3) Subsidence not apparent in any one direction, where the SDE was circular in shape, demonstrating that the subsidence was distributed in all directions.

The study utilized the SDE method to investigate subsidence patterns, categorizing them into three levels based on cumulative subsidence values. Analysis revealed spatial variations over time, with 2017 showing uniform subsidence in all directions, 2018 displaying intensified subsidence in the north-south direction, and 2019 witnessing a shift towards southeast-northwest direction for high-level subsidence. By 2020, patterns resembled those of 2019, while 2021 saw an east-west alignment indicating a shift in subsidence occurrence. In 2022, subsidence spread out diffusely. These findings illuminate temporal and spatial subsidence fluctuations in the study area.

6. Acknowledgements

This research was supported in part by the Graduate Program Scholarship from The Graduate School, Kasetsart University, Bangkok, Thailand.

7. References

- Aobpaet, A., Cuenca, M. C., Hooper, A., & Trisirisatayawong, I. (2013). InSAR time-series analysis of land subsidence in Bangkok, Thailand. *International Journal of Remote Sensing*, 34(8), 2969-2982.
<https://doi.org/10.1080/01431161.2012.756596>
- Babel, M. S., Gupta, A. D., Domingo, N. D. S., & Donna, N. (2006). Land subsidence: A consequence of groundwater over-exploitation in Bangkok, Thailand. *International Review for Environmental Strategies*, 6(2), 307-327.
- Cigna, F., Esquivel Ramírez, R., & Tapete, D. (2021). Accuracy of Sentinel-1 PSI and SBAS InSAR Displacement Velocities against GNSS and Geodetic Leveling Monitoring Data. *Remote Sensing*, 13(23), 1-28.
<https://doi.org/10.3390/rs13234800>
- Department of Groundwater Resources. (2012). *Report on the groundwater situation in Thailand 2012. Department of Groundwater Resources Report*. Retrieved 07 06, 2023 from <https://disastervru.wordpress.com/wp-content/uploads/2019/03/e0b8a3e0b8b2e0b8a2e0b887e0b8b2e0b899e0b8aae0b896e0b8b2e0b899e0b881e0b8b2e0b8a3e0b893e0b98ce0b899e0b989e0b8b3e0b89ae0b8b2e0b894e0b8b2e0b8a52555.pdf>
- Ding, X. L., Li, Z. W., Zhu, J. J., Feng, G. C., & Long, J. P. (2008). Atmospheric effects on InSAR measurements and their mitigation. *Sensors*, 8(9), 5426-5448.
<https://doi.org/10.3390/s8095426>
- Dumka, R. K., SuriBabu, D., Malik, K., Prajapati, S., & Narain, P. (2020). PS-InSAR derived deformation study in the Kachchh, Western India. *Applied Computing and Geosciences*, 8, Article 100041.
<https://doi.org/10.1016/j.acags.2020.100041>
- Ferretti, A., Prati, C., & Rocca, F. (2001). Permanent scatterers in SAR interferometry. *IEEE Transactions on Geoscience and Remote Sensing*, 39(1), 8-20.
<https://doi.org/10.1109/36.898661>
- Foumelis, M., Blasco, J. M. D., Desnos, Y. L., Engdahl, M., Fernández, D., Veci, L., ... & Wong, C. (2018, July 22-27). *ESA SNAP-StaMPS integrated processing for Sentinel-1 persistent scatterer interferometry* [Conference presentation]. *IGARSS 2018-2018 IEEE International Geoscience and Remote Sensing Symposium*. IEEE. Valencia, Spain.
<https://doi.org/10.1109/igarss.2018.8519545>
- Fuhrmann, T., Caro Cuenca, M., Knöpfler, A., Van Leijen, F. J., Mayer, M., Westerhaus, M., ... & Heck, B. (2015). Estimation of small surface displacements in the Upper Rhine Graben area from a combined analysis of PS-InSAR, levelling and GNSS data. *Geophysical Journal International*, 203(1), 614-631.
<https://doi.org/10.1093/gji/ggv328>

- Gatsios, T., Cigna, F., Tapete, D., Sakkas, V., Pavlou, K., & Parcharidis, I. (2020). Copernicus sentinel-1 MT-InSAR, GNSS and seismic monitoring of deformation patterns and trends at the Methana Volcano, Greece. *Applied Sciences*, 10(18), 1-23. <https://doi.org/10.3390/app10186445>
- Guo, L., Gong, H., Ke, Y., Zhu, L., Li, X., Lyu, M., & Zhang, K. (2021). Mechanism of land subsidence mutation in Beijing plain under the background of urban expansion. *Remote Sensing*, 13(16), 1-22. <https://doi.org/10.3390/rs13163086>
- Hooper, A., Zebker, H., Segall, P., & Kampes, B. (2004). A new method for measuring deformation on volcanoes and other natural terrains using InSAR persistent scatterers. *Geophysical Research Letters*, 31(23), 1-5. <https://doi.org/10.1029/2004gl021737>
- Hussain, M. A., Chen, Z., Wang, R., & Shoaib, M. (2021). PS-InSAR-based validated landslide susceptibility mapping along Karakorum Highway, Pakistan. *Remote Sensing*, 13(20), 1-25. <https://doi.org/10.3390/rs13204129>
- Jennifer, J. J., Saravanan, S., & Pradhan, B. (2022). Persistent Scatterer Interferometry in the post-event monitoring of the Idukki Landslides. *Geocarto International*, 37(5), 1514-1528. <https://doi.org/10.1080/10106049.2020.1778101>
- Khan, J., Ren, X., Hussain, M. A., & Jan, M. Q. (2022). Monitoring land subsidence using PS-InSAR technique in Rawalpindi and islamabad, Pakistan. *Remote Sensing*, 14(15), 1-25. <https://doi.org/10.3390/rs14153722>
- Kun, F., Margane, A., Tatonc, T., & Wever, T. (2004) InSAR-Based Land Subsidence Map for Bangkok, Thailand. *Zeitschrift Fur Angewandte Geologie*, 50(1), 74-81.
- Lefever, D. W. (1926). Measuring geographic concentration by means of the standard deviational ellipse. *American Journal of Sociology*, 32(1), 88-94. <https://doi.org/10.1086/214027>
- Li, H., Zhu, L., Dai, Z., Gong, H., Guo, T., Guo, G., ... & Teatini, P. (2021). Spatiotemporal modeling of land subsidence using a geographically weighted deep learning method based on PS-InSAR. *Science of The Total Environment*, 799, Article 149244. <https://doi.org/10.1016/j.scitotenv.2021.149244>
- Li, Y., Gong, H., Zhu, L., & Li, X. (2017). Measuring spatiotemporal features of land subsidence, groundwater drawdown, and compressible layer thickness in Beijing Plain, China. *Water*, 9(1), 1-17. <https://doi.org/10.3390/w9010064>
- Lu, Z., Kwoun, O., & Rykhus, R. (2007). Interferometric synthetic aperture radar (InSAR): its past, present and future. *Photogrammetric Engineering and Remote Sensing*, 73(3), 217-221. <https://doi.org/10.1201/9781420094428-c2>
- Peng, J., Chen, S., Lü, H., Liu, Y., & Wu, J. (2016). Spatiotemporal patterns of remotely sensed PM2.5 concentration in China from 1999 to 2011. *Remote Sensing of Environment*, 174, 109-121. <https://doi.org/10.1016/j.rse.2015.12.008>
- Phien-Wej, N., Giao, P. H., & Nutalaya, P. (2006). Land subsidence in bangkok, Thailand. *Engineering Geology*, 82(4), 187-201. <https://doi.org/10.1016/j.enggeo.2005.10.004>
- Pritchard, M. E., & Simons, M. (2004). An InSAR-based survey of volcanic deformation in the southern Andes. *Geophysical Research Letters*, 31(15), 1-4. <https://doi.org/10.1029/2004gl020545>
- Ramirez, R. A., Lee, G. J., Choi, S. K., Kwon, T. H., Kim, Y. C., Ryu, H. H., ... & Hyun, C. (2022). Monitoring of construction-induced urban ground deformations using Sentinel-1 PS-InSAR: The case study of tunneling in Dangjin, Korea. *International Journal of Applied Earth Observation and Geoinformation*, 108, Article 102721. <https://doi.org/10.1016/j.jag.2022.102721>
- Rosen, P. A., Hensley, S., Joughin, I. R., Li, F. K., Madsen, S. N., Rodriguez, E., & Goldstein, R. M. (2000). Synthetic aperture radar interferometry. *Proceedings of the IEEE*, 88(3), 333-382. <https://doi.org/10.1109/5.838084>
- Rosi, A., Tofani, V., Tanteri, L., Tacconi Stefanelli, C., Agostini, A., Catani, F., & Casagli, N. (2018). The new landslide inventory of Tuscany (Italy) updated with PS-InSAR: geomorphological features and landslide distribution. *Landslides*, 15, 5-19. <https://doi.org/10.1007/s10346-017-0861-4>
- Sousa, J. J., Hooper, A. J., Hanssen, R. F., Bastos, L. C., & Ruiz, A. M. (2011). Persistent Scatterer

- InSAR: A comparison of methodologies based on a model of temporal deformation vs. spatial correlation selection criteria. *Remote Sensing of Environment*, 115(10), 2652-2663.
<https://doi.org/10.1016/j.rse.2011.05.021>
- Sousa, J. J., Ruiz, A. M., Hanssen, R. F., Perski, Z., Bastos, L., Gil, A. J., & Galindo-Zaldívar, J. (2008). PS-INSAR measurement of ground subsidence in Granada area (Betic Cordillera, Spain). *Proceedings of 13th FIG Deformation Measurement and Analysis, LNEC, Lisbon*, 12-15.
<https://doi.org/10.1016/j.protcy.2014.10.040>
- Sun, H., Zhang, Q., Zhao, C., Yang, C., Sun, Q., & Chen, W. (2017). Monitoring land subsidence in the southern part of the lower Liaohe plain, China with a multi-track PS-InSAR technique. *Remote Sensing of Environment*, 188, 73-84.
<https://doi.org/10.1016/j.rse.2016.10.037>
- Sun, Q., Zhang, L., Ding, X. L., Hu, J., Li, Z. W., & Zhu, J. J. (2015). Slope deformation prior to Zhouqu, China landslide from InSAR time series analysis. *Remote Sensing of Environment*, 156, 45-57.
<https://doi.org/10.1016/j.rse.2014.09.029>
- Yang, K., Yan, L., Huang, G., Chen, C., & Wu, Z. (2016). Monitoring building deformation with InSAR: Experiments and validation. *Sensors*, 16(12), 1-16.
<https://doi.org/10.3390/s16122182>
- Zuo, J., Gong, H., Chen, B., Liu, K., Zhou, C., & Ke, Y. (2019). Time-series evolution patterns of land subsidence in the eastern Beijing Plain, China. *Remote Sensing*, 11(5), 1-19.
<https://doi.org/10.3390/s16122182>